Journal of Power Sources 193 (2009) 747–753

Contents lists available at ScienceDirect

Journal of Power Sources

journal homepage: www.elsevier.com/locate/jpowsour

Solid oxide fuel cell cathodes prepared by infiltration of $LaNi_{0.6}Fe_{0.4}O_3$ and $La_{0.91}Sr_{0.09}Ni_{0.6}Fe_{0.4}O_3$ in porous yttria-stabilized zirconia

Shiwoo Lee[a], M. Bevilacqua[b], P. Fornasiero[b], J.M. Vohs[a], R.J. Gorte[a,*]

[a] Department of Chemical and Biomolecular Engineering, University of Pennsylvania, Philadelphia, PA 19104, USA
[b] Chemistry Department, ICCOM CNR, and INSTM-Trieste, University of Trieste, via L. Giorgieri 1, I-34127 Trieste, Italy

ARTICLE INFO

Article history:
Received 17 March 2009
Received in revised form 21 April 2009
Accepted 22 April 2009
Available online 3 May 2009

Keywords:
Solid oxide fuel cells
Yttria-stabilized zirconia
Cathodes
Lanthanum ferrite
Lanthanum nickel ferrite
Ionic conductivity

ABSTRACT

SOFC composite electrodes of yttria-stabilized zirconia (YSZ) and either $LaNi_{0.6}Fe_{0.4}O_3$ (LNF) or $La_{0.91}Sr_{0.09}Ni_{0.6}Fe_{0.4}O_3$ (LSNF) were prepared by infiltration to a loading of 40 wt% of the perovskite into porous YSZ using aqueous solutions of the nitrate salts. XRD measurements indicated that the perovskite structures were formed following calcination at 850 °C, at which temperature the LNF and LSNF form small particles that coat the YSZ pores. Heating to 1100 °C causes the particles to form a dense film over the YSZ but caused no solid-state reaction. Calcination of an LNF–YSZ composite to 1200 °C led to an expansion of the LNF lattice, suggesting introduction of Zr(IV) into the perovskite; further heating to 1300 °C caused the formation of $La_2Zr_2O_7$. For 850 °C calcination, the electrode performance of both LNF–YSZ and LSNF–YSZ composites was similar to that reported for composites of YSZ and $La_{0.8}Sr_{0.2}FeO_3$ (LSF), with a current-independent impedance of approximately 0.1 Ω cm^2 at 700 °C in air. For 1100 °C calcination, both LNF–YSZ and LSNF–YSZ composites exhibited impedances that decreased strongly under both anodic and cathodic polarization. The implications of these results for preparing electrodes based on LNF and LSNF are discussed.

1. Introduction

The performance-limiting factor in solid oxide fuel cells (SOFC) is often the cathode impedance [1–3]. This is because the standard cathode material with yttria-stabilized zirconia (YSZ) electrolytes is still a composite of Sr-doped $LaMnO_3$ (LSM) and YSZ, despite the fact that LSM–YSZ cathodes have relatively high impedances at temperatures below 750 °C [4]. The impedance of cathodes made from mixed-conducting perovskites, such as Sr-doped $LaCoO_3$ (LSCo) [5–8], $LaFeO_3$ (LSF) [9–12], or $LaFe_{0.8}Co_{0.2}O_3$ (LSCF) [13,14], can be much lower; however, the preparation of these alternative electrodes is complicated by the fact that many of the mixed-conducting perovskites undergo a solid-state reaction with YSZ at the sintering temperatures required for standard preparation of SOFC electrodes.

The formation of insulating phases during electrode fabrication can be avoided by using low-temperature, infiltration procedures to synthesize the electrodes [15–17]. This procedure involves preparing a porous YSZ scaffold together with the electrolyte, then infiltrating either the perovskite nanoparticles or the precursor salts required to form the perovskites within the scaffold. Because the procedure allows formation of a long three-phase boundary (TPB), the initial performance of these electrodes can be quite good. Unfortunately, stability has remained a problem. Since solid-state reaction between LSCo and YSZ occurs already at the 700 °C [18], it is not surprising that electrodes formed by infiltration with LSCo are not stable [15,19]. By comparison, LSF and YSZ are relatively unreactive, with no evidence for interfacial reactions even at 1100 °C [9,20,21]. A major problem with LSF is its relatively low electronic conductivity, on the order of 50 S cm^{-1}, compared to 200 S cm^{-1} for LSM. Since the conductivities of composites formed by infiltration of a conductor into an insulating scaffold are typically 100 times lower than the intrinsic conductivity of the pure conductor [16], this lower conductivity can be a serious issue. The usual approach to increasing the conductivity of LSF is to dope with Co (i.e., form LSCF) but this likely re-introduces the problem of reactivity between Co and YSZ.

Our groups have recently investigated the properties of perovskites based on Fe and Ni, $LaNi_{0.6}Fe_{0.4}O_{3-\delta}$ (LNF) and $La_{1-x}Sr_xNi_{0.6}Fe_{0.4}O_3$ (LSNF) [22–24]. The fact that NiO can be co-sintered with YSZ in the formation Ni-YSZ anodes (Co-sintering of CoO_x and YSZ is not possible due diffusion of CoO_x into YSZ [25]) suggests that LNF and LSNF are likely to be significantly less reactive with YSZ than is LSCF. The conductivity of even pure LNF is high, similar to that of LSM and LSCF, and can be further enhanced by doping with Sr, with a maximum electronic conductivity at $x = 0.09$

* Corresponding author at: Department of Chemical and Biomolecular Engineering, University of Pennsylvania, 311 Towne Building, 220 South 33rd Street, Philadelphia, PA 19104, USA. Tel.: +1 215 898 4439; fax: +1 215 573 2093.
E-mail address: gorte@seas.upenn.edu (R.J. Gorte).

0378-7753/$ – see front matter © 2009 Elsevier B.V. All rights reserved.
doi:10.1016/j.jpowsour.2009.04.046

Table 1
Electrical and Ionic Conductivities of LNF, LSNF and LSF at 700 °C.

	LNF	LSNF	LSF
Electrical conductivity (S cm^{-1})	235	385	80
Ionic conductivity (S cm^{-1})	1.6×10^{-6}	4.9×10^{-5}	8.3×10^{-4}

of almost 400 S cm^{-1} in air at 700 °C [24]. The ionic conductivity of LSNF at this composition is about 20 times lower than that of LSF but higher than that of LNF by a factor of 30. The electronic and ionic conductivities of $La_{0.8}Sr_{0.2}FeO_3$ (LSF), $LaNi_{0.6}Fe_{0.4}O_3$ (LNF), and $La_{0.91}Sr_{0.09}Ni_{0.6}Fe_{0.4}O_3$ (LSNF) at 700 °C are summarized in Table 1.

LNF–YSZ cathodes prepared by conventional methods do exhibit some desirable properties but overall electrode performance is not comparable to that of LSM–YSZ electrodes. Regarding good properties, LNF exhibits reasonable compatibility for thermal expansion with traditional electrolyte materials [26] and appears to be more tolerant towards Cr poisoning, associated with stainless steel interconnects, than are cathodes based on LSM [27,28]. However, electrode impedances tend to be high, at least in part due to formation of $La_2Zr_2O_7$ [29]. Although one study achieved a power density of 1.56 W cm^{-2} at 800 °C with an LNF cathode and a zirconia-based electrolyte [30], it was necessary to polarize the electrode at high current densities for long times to achieve this. In other studies, reasonable performances were reported by placing a thin layer of Sm-doped ceria (SDC) between the LNF and the electrolyte or by using an LNF–SDC composite as the electrode [31]. In both cases, however, the cathode impedances were inconsistent with fuel-cell power densities greater than 1 W cm^{-2} at 800 °C. Finally, Simner et al. compared cathodes based on $La_{0.8}Sr_{0.2}FeO_{3-\delta}$, $La_{0.7}Sr_{0.3}Fe_{0.8}Ni_{0.2}O_{3-\delta}$, and $LaNi_{0.6}Fe_{0.4}O_{3-\delta}$ and found LSF to give the best performance [10]. In agreement with this, a later study examined a series of LSNF cathodes and reported that increasing Ni content decreased performance [32].

In the present paper, we compare the performance of LSF, LNF, and LSNF cathodes prepared by infiltration into porous YSZ. For calcination at 850 °C, each of the perovskites formed nanoparticle coatings over the YSZ scaffold and each provided similar electrode impedances that were independent of current density. After calcination to 1100 °C, each of the perovskites appeared to form a dense coating over the YSZ scaffold. The high-temperature electrodes exhibited impedances that were highly current-dependent. The curvature was much more pronounced with the LNF and LSNF electrodes, possibly due to their lower ionic conductivity compared to LSF.

2. Experimental

The fuel-cell, composite electrodes were prepared using infiltration procedures similar to those described in earlier papers [20,33–35]. The first step in fuel-cell preparation involved making a YSZ wafer that had a dense layer between two porous layers. The porous-dense-porous YSZ structure was produced by laminating three green tapes, using graphite as the pore former in the layers that were to be porous, and then firing the structure to 1500 °C for 4 h. The green tapes were prepared by mixing YSZ powder (Tosoh Corp., 8 mol% Y_2O_3-doped ZrO_2, 0.2 μm) with distilled water, a dispersant (Duramax 3005, Rohm & Haas), and binders (HA12 and B1000, Rohm & Haas). In the present study, the dense electrolyte layers were between 80 and 100 μm thick and had a diameter of 1 cm, while the two porous layers were each 50 μm thick and 0.67 cm in diameter. Based on earlier work, the porous layers were known to be 65% porous and have relatively uniform pore dimensions between 1 and 2 μm [36].

Either LNF or LNSF was incorporated into porous YSZ by infiltration with aqueous solutions containing $La(NO_3)_3{\cdot}6H_2O$, $Fe(NO_3)_3{\cdot}9H_2O$, $Ni(NO_3)_2{\cdot}6H_2O$, and $Sr(NO_3)_2$ at the proper molar ratios. After infiltration, the salts were calcined in air to 450 °C for 30 min to decompose the nitrate ions and then re-infiltrated with the salt solutions until the desired loading, 40 wt% of the added oxide, was achieved. To form the perovskite phases, the mixed oxides were heated in air to either 850 or 1100 °C with a heating rate of 3 °C min^{-1} for 4 h. For symmetric-cell measurements, both porous layers of the porous-dense-porous YSZ structure were infiltrated simultaneously. For fuel-cell measurements, the anodes were prepared after forming the LNF or LSNF cathode. The anodes were formed by infiltration of 40 wt% ceria and 0.5 wt% Pd. The ceria was added first, using an aqueous solution of $Ce(NO_3)_3{\cdot}6H_2O$ and calcination to 850 °C with a heating rate of 3 °C min^{-1} for 4 h, after which the Pd was added using $(NH_3)_4Pd(NO_3)_2$ and calcination at 450 °C for 30 min. Based on earlier studies [37–39], an anode of this composition contributes about 0.1 Ω cm^2 to the non-ohmic impedance of cells operating at 700 °C in humidified H_2. Because we have found the use of reference electrodes to be unreliable [40], cathode performance in this paper was estimated from the total-cell performance by subtracting the contribution of the above anode losses and checked using symmetric cells.

For fuel-cell testing, the cells were attached to an alumina tube with a ceramic adhesive (Aremco, Ceramabond 552). Ag paste was used as the current collector under both air and fuel conditions. Impedance spectra were measured at open circuit in the galvanostatic mode with a frequency range of 0.1 Hz to 100 KHz and a 1 mA AC perturbation using a Gamry Instruments potentiostat. H_2 was introduced to the anode compartment at a flow rate of 50 ml min^{-1} through a room-temperature, water bubbler for humidification.

The physical characteristics of the cathode composites were examined by XRD using Cu Kα radiation, to ensure that the proper phases were produced, and by scanning electron microscopy (JEOL 5600 SEM). For the atomic force microscopy (AFM) measurements, an aqueous solution of $La(NO_3)_3{\cdot}6H_2O$, $Fe(NO_3)_3{\cdot}9H_2O$, and $Ni(NO_3)_2{\cdot}6H_2O$ was prepared in the proper stoichiometry to form LNF. This solution was then sprayed onto a heated YSZ(1 0 0) crystal. Deposited specimens were heat-treated at various temperatures for 4 h. The topology of the deposited particles was then investigated using AFM (Pacific Nanotechnology Inc.).

3. Results

In order to characterize the phases formed by infiltration of the nitrate salts, followed by calcination to various temperatures, XRD measurements were performed. Figs. 1 and 2 provide this data for the addition of 40 wt% of oxides with the stoichiometries of either LNF or LSNF into the porous YSZ. For LNF, the pattern obtained after heating to 850 °C, Fig. 1a, shows a very broad peak centered at approximately 32.8° 2θ. It has previously been reported that the diffraction pattern for LNF in this region shows splitting of the main reflection, due to the tilting of the octahedra constituting the perovskite with respect to the c axis, so that there are two peaks at 32.6 and 32.9° 2θ [24,41]. The pattern at 850 °C is consistent with the formation of very small crystallites, which in turn causes sufficient broadening that the two peaks are not resolved.

With increasing calcination temperature, the peak corresponding to the LNF perovskite narrows and shifts to lower angles. By 1200 °C, Fig. 1c, the peak has shifted to 32.2° 2θ. The results here are reminiscent of those reported for LSF–YSZ composites, where a similar shift in the peak associated with the perovskite occurs at approximately the same temperatures seen here [20,21]. In the LSF–YSZ case, the shift in the diffraction peak to lower angles is believed to be caused by the incorporation of Zr(IV) into the B sites of the perovskite [21]. Therefore, we suggest that incorpora-

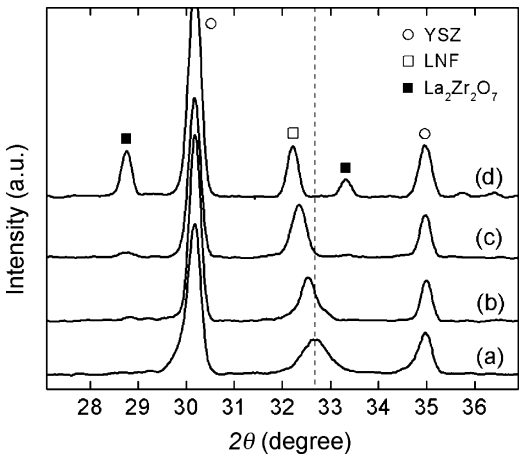

Fig. 1. XRD patterns of the LNF–YSZ composite calcined to (a) 850 °C, (b) 1100 °C, (c) 1200 °C, and (d) 1300 °C.

tion of Zr(IV) also occurs in LNF at higher calcination temperatures. While substitution of Zr(IV) into the perovskite structure could lead to deactivation, Wang et al. obtained reasonable electrode performance using a composite $La_{0.8}Sr_{0.2}Fe_{0.9}Zr_{0.1}O_3$ and YSZ formed by infiltration [20].

When the composite is heated to 1300 °C, the diffraction pattern shows the formation of $La_2Zr_2O_7$. Since formation of $La_2Zr_2O_7$ can occur even with LSM–YSZ composites at these elevated temperatures [42], it is perhaps more significant to notice that formation of $La_2Zr_2O_7$ appears to be insignificant at lower temperatures. In particular, there is no evidence for the formation of insulating phases following calcination at 1100 °C. Since a previous study of LSF–YSZ composites suggested that the effects of calcination at 1100 °C mimicked that observed following operation for long times at 700 and 800 °C [20], the fact that there is no evidence for $La_2Zr_2O_7$ and minimal shift in the XRD peak for the perovskite in Fig. 1b implies that solid-state reactions may not be a problem for LNF–YSZ electrodes under practical conditions.

Fig. 2 shows the XRD patterns analogous to those in Fig. 1 but following infiltration of an oxide with the stoichiometry of LSNF. While the diffraction peaks for LSNF are broader than those observed for LNF at each temperature, the general conclusions for LSNF are the same. There is again a shift in the perovskite peak to lower angles with increasing calcination temperature, suggesting Zr(IV) incorporation into the lattice. The formation of $La_2Zr_2O_7$ occurs following calcination at 1300 °C but is not formed at lower temperatures.

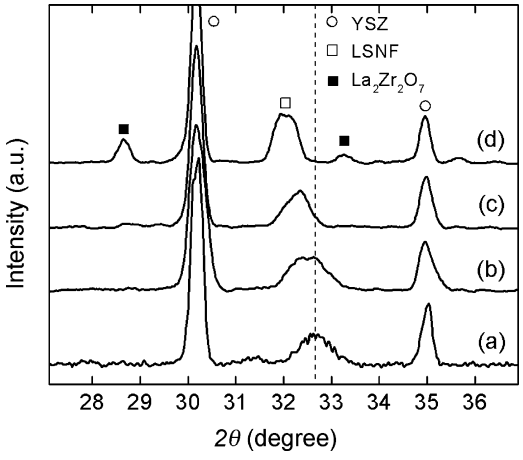

Fig. 2. XRD patterns of the LSNF–YSZ composite calcined to (a) 850 °C, (b) 1100 °C, (c) 1200 °C, and (d) 1300 °C.

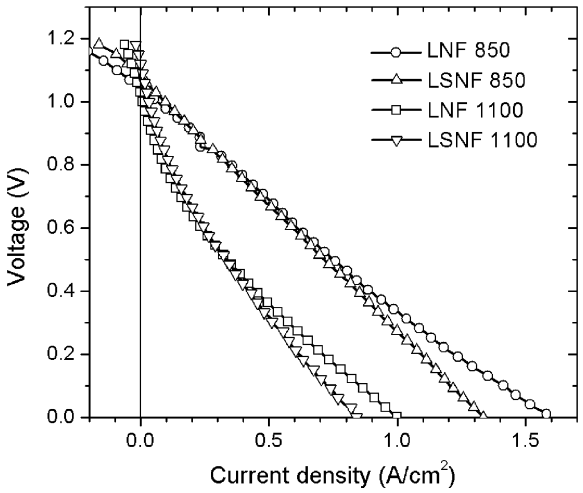

Fig. 3. *V–I* polarization curves for fuel cells with LNF–YSZ and LSNF–YSZ composite cathode calcined at 850 and 1100 °C.

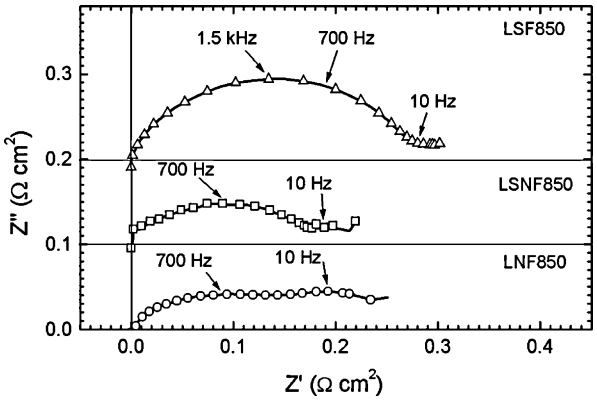

Fig. 4. Cole–Cole plots for the cells with LNF–YSZ, LSNF–YSZ, and LSF–YSZ cathodes calcined to 850 °C. The measurements were performed at open circuit holding the cathodes in air at 700 °C.

The effect of calcination temperature and electrode composition on fuel-cell performance at 700 °C is shown by the data in Figs. 3–5. Fig. 3 shows *V–I* polarization curves for fuel cells with LNF–YSZ and LSNF–YSZ cathodes that had been calcined at 850 and 1100 °C. In

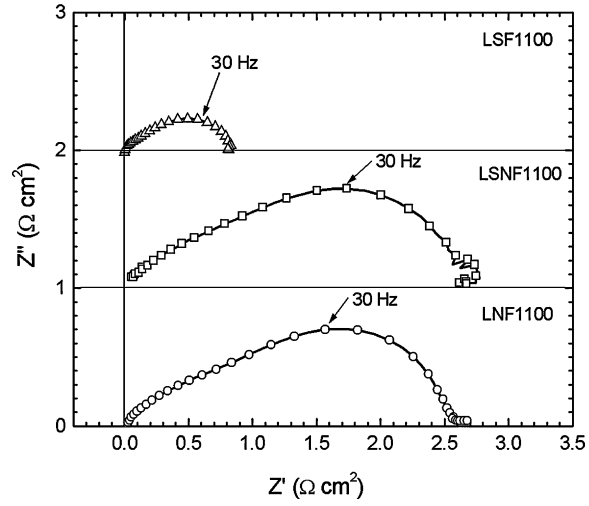

Fig. 5. Cole–Cole plots for the cells with LNF–YSZ, LSNF–YSZ, and LSF–YSZ cathodes calcined to 1100 °C. The measurements were performed at open circuit holding the cathodes in air at 700 °C.

each of these cells, the electrolyte thicknesses were approximately 90 μm and the anodes were exactly the same, 0.5 wt% Pd and 40 wt% ceria infiltrated into porous YSZ. In each measurement, humidified (3% H_2O) H_2 was admitted to the anode chamber and the cathodes were simply exposed to air. First, it is apparent that the performance characteristics of the LNF–YSZ and LSNF–YSZ cathodes are identical. Following calcination at 850 °C, the *V–I* relationships for both LNF and LSNF form a nearly straight line, while the *V–I* relationships for both electrode compositions are highly curved, concave upward, following calcination at 1100 °C. Therefore, the change in the morphology/nanostructure of the nanocomposite induced by the calcination temperature, not the composition, is the main factor in determining the performance.

The performance level of the electrodes that were calcined to 850 °C is quite good, as shown by the *V–I* relationships and the impedance data in Fig. 4. The open-circuit impedance data for the two cells operating in air at 700 °C, reported in Fig. 4 with the ohmic resistances removed, are nearly identical and similar to that measured on a cell with an LSF–YSZ composite cathode using the same cell configuration and anode [34]. The total non-ohmic losses in all three cells varied between 0.22 and 0.30 Ω cm^2. Since an earlier estimate of anode losses for 40 wt% ceria and 0.5 wt% Pd formed by infiltration was 0.1 Ω cm^2, the cathode losses for the LNF–YSZ and LSNF–YSZ electrodes were also approximately 0.1 Ω cm^2, the same value reported for LSF–YSZ electrodes [20,34]. Finally, it should be noted that the impedance measurements are consistent with the *V–I* data in Fig. 3. Based on the slope of the *V–I* data, the total area-specific resistances for the cells calcined to 850 °C were between 0.7 and 0.75 Ω cm^2. Since a 90 μm YSZ electrolyte is expected to have an ohmic contribution of 0.48 Ω cm^2, the total electrode contributions must be between 0.2 and 0.3 Ω cm^2. Because the *V–I* relationship is a straight line, the impedance of the cathodes calcined to 850 °C is independent of current density.

Both the LNF–YSZ and LSNF–YSZ electrodes show significant curvature following calcination at 1100 °C. Since the slopes at high current densities are nearly the same as that observed with the cathodes calcined at 850 °C, the ohmic losses were unchanged. This was confirmed by the impedance measurements, which also showed that the non-ohmic losses were large and highly dependent on the current density after calcination at 1100 °C. The open-circuit impedance data for these two cells are reported in Fig. 5, together with data from an LSF–YSZ cell treated in the same manner. Again, the results for the fuel cells with LNF–YSZ and LSNF–YSZ electrodes are identical, with both showing non-ohmic losses of greater than 2.5 Ω cm^2 at 700 °C; however, the LSF–YSZ electrode was affected much less. While the LSF–YSZ electrode also showed significantly higher impedances and current dependence after heating in air to 1100 °C, the effect was less pronounced. As demonstrated in Fig. 5, the total non-ohmic impedance of a similar cell with an LSF–YSZ electrode was only 1.0 Ω cm^2 at open circuit.

To investigate the electrochemical properties of the LNF–YSZ and LSNF–YSZ electrodes further, we prepared symmetric cells from the same porous-dense-porous YSZ wafers that were used to synthesize the fuel cells. Since these measurements simply confirmed what was reported in the fuel-cell measurements, we show only a summary of the data for the cell with LNF–YSZ electrodes that had been calcined to 1100 °C. Fig. 6 reports the ohmic and non-ohmic losses for this cell as a function of current density, for operation at 700 °C in air. As expected the ohmic losses were independent of current density and in good agreement with the value calculated for the 90-μm YSZ electrolyte, 0.5 Ω cm^2. The total non-ohmic loss at open circuit was initially 5.0 Ω cm^2, twice the value estimated for a single LNF–YSZ electrode from Fig. 5. The non-ohmic losses are found to be strongly dependent on current density, approaching a value of 0.2 Ω cm^2 for current densities above 1.0 A cm^{-2}. After polarizing the cell by passing a positive current, the total non-ohmic impedance at open circuit decreased to 3.2 Ω cm^2. This is similar to what is observed with symmetric cells made from LSM–YSZ and indicates hysteretic behavior [43]. Finally, it is noteworthy that the impedance at high positive or negative current densities was the same, 0.2 Ω cm^2, a value that is also approximately twice the impedance estimated for the LNF–YSZ electrode calcined to 850 °C.

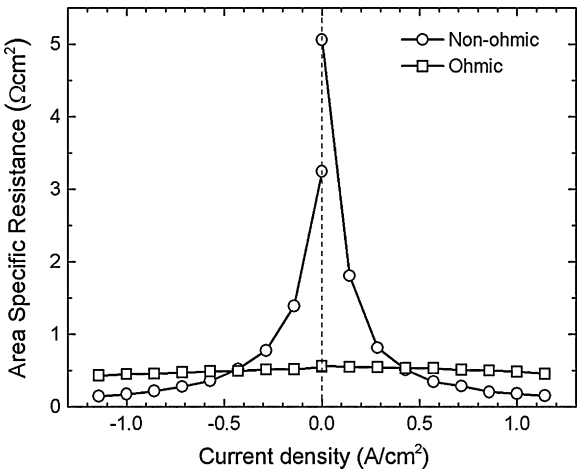

Fig. 6. Plots of the ohmic and non-ohmic impedances of a symmetric cell with LNF–YSZ electrodes calcined to 1100 °C as a function of current density.

The one new piece of information from Fig. 6 that was not indicated by the fuel-cell performance is that the impedances of the LNF–YSZ electrodes decrease with current density in the same manner for anodic and cathodic polarization. The cell is obviously no longer symmetric when current is applied. Since the impedance is very low at high current densities, the impedance of both electrodes must be affected in a similar manner. Again, this is similar to what was observed with LSF–YSZ in a previous study. The classical explanation for current-dependent impedances is that the electrode overpotential assists in making the reactants overcome the activation barrier, as described by Butler–Volmer kinetics; however, it is difficult to understand how the barrier would be the same for both cathodic and anodic reactions. The *V–I* relationship also does not follow the exponential dependence predicted by Butler–Volmer kinetics [20].

To understand the changes that occur upon calcination to 1100 °C, we examined the electrodes by SEM. Fig. 7a is a micrograph of the porous YSZ scaffold. As mentioned earlier, the scaffold has a "sponge-like" appearance, with channels that are typically between 1 and 2 μm in diameter. Fig. 7b and c are images of the scaffold after adding 40 wt% of either LNF or LSNF and heating in air to 850 °C. In both cases, the LNF and LSNF are present as small particles, approximately 0.1–0.2 μm in size, that form a porous coating over the YSZ structure. When the LNF and LSNF were heated to 1100 °C, the porous perovskite coatings appear to become dense. This is again similar to what was observed with Sr-, Ba-, and Ca-doped $LaFeO_3$ [20,34].

Finally, to understand the processes that drive the change in perovskite-particle morphology, we examined the effect of calcination temperature on small particles of LNF deposited onto a YSZ(1 0 0) crystal using AFM, with the results shown in Fig. 8. Fig. 8a shows a micrograph of particles following calcination to 1000 °C. The surface of the crystal is covered with a uniform distribution of particles, roughly 20–30 nm in diameter, with heights that are typically 4–6 nm. When this surface was heated to 1100 °C, the particles appeared to spread out and form a relatively uniform film over the YSZ. This is similar to what was observed with LSM particles on YSZ crystals [44,45]. In that case, it was suggested that surface interactions (e.g. "wetting" interactions) between the perovskite and the

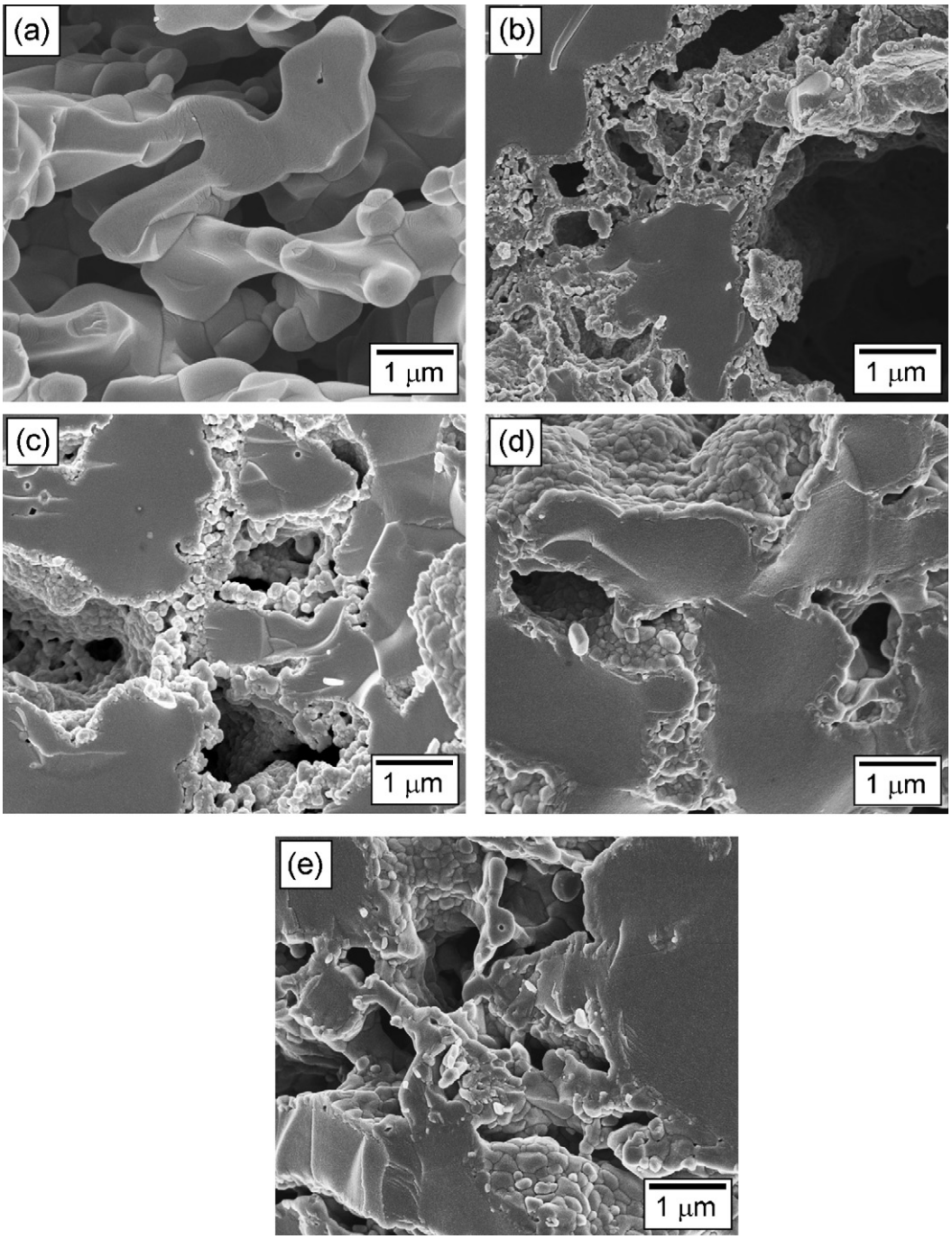

Fig. 7. SEM images of (a) the YSZ backbone, (b) the LNF–YSZ composite calcined to 850 °C, (c) the LSNF–YSZ composite calcined to 850 °C, (d) the LNF–YSZ composite calcined to 1100 °C, and (e) the LSNF–YSZ composite calcined to 1100 °C.

YSZ provided a driving force for causing the particles to spread. Based on the results in Fig. 8, it would appear that similar effects may be occurring with LNF and YSZ, causing the perovskite to coat the pores of the YSZ.

4. Discussion

One of our groups has recently investigated the properties of SOFC cathodes prepared by infiltration of Sr-, Ba-, and Ca-doped $LaFeO_3$ (LSF, LBF, and LCF) [34]. What is remarkable about the present results with LNF and LSNF is how similar the electrochemical properties of all of these materials are. Based on XRD results, all of these perovskites were unreactive with YSZ up to at least 1100 °C. Following calcination to 850 °C, each of the infiltrated cathodes exhibited a current-independent impedance of approximately 0.1 $\Omega\,cm^2$ at 700 °C in air. Following calcination to 1100 °C, the impedances at 700 °C of each of the infiltrated cathodes were much higher, but the impedances decreased sharply with current density, independent of the sign of that current, whether anodic or cathodic. In each case, the changes in the electrochemical performance with increasing calcination temperature were accompanied by the formation of a film-like coating of the perovskite over the YSZ pore structure.

It is interesting to ask how the electrochemical properties are affected by the materials properties. The addition of Ni to the perovskite (LSF to LSNF) increases the electronic conductivity by a

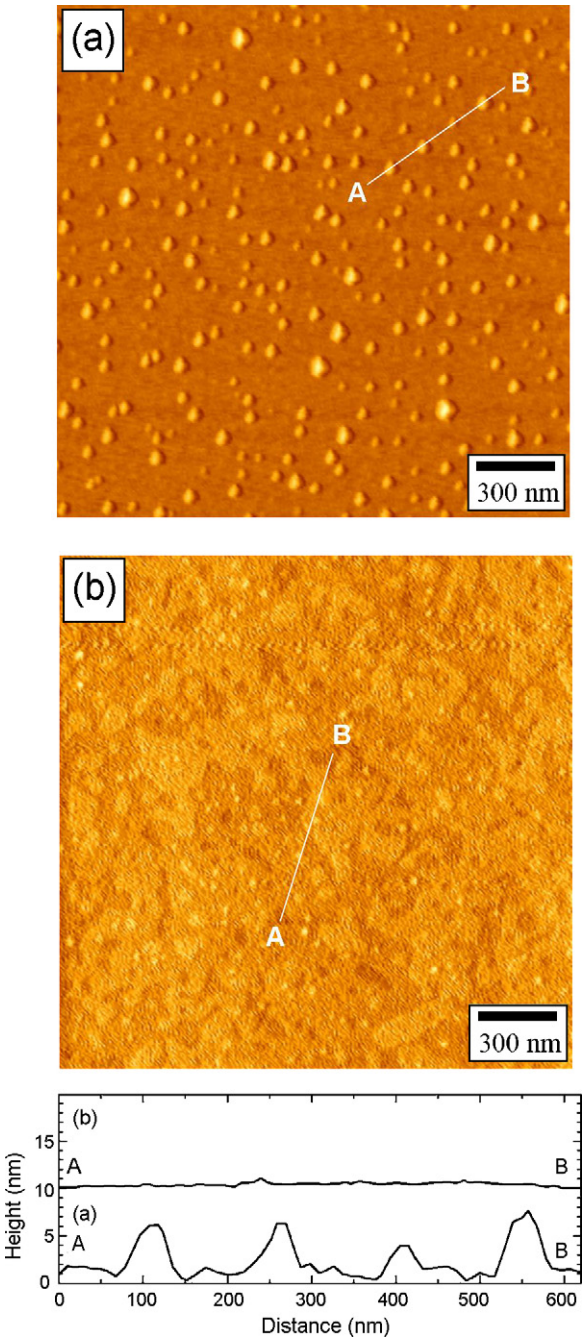

Fig. 8. AFM images of LNF particles on a YSZ(1 0 0) single crystal after calcination to (a) 1000 °C and (b) 1100 °C. Height profiles were drawn along the lines A to B.

factor of 5 but at the cost of losing more than an order of magnitude in the ionic conductivity. Similarly, the substitution of Ca for Sr (LSF to LCF) has little impact on electronic conductivity but also decreases ionic conductivity by a more than an order of magnitude. For calcination at the lower temperatures, conditions for which the perovskite phase forms a layer over the YSZ structure that is highly porous, changes in ionic and electronic conductivity seem to have no impact on electrode performance. It is only following treatment at higher temperatures, where the perovskites appear to form a film over the YSZ, that we observe differences between the various materials. Even then, the differences between the LNF, LSNF, LSF, LBF, and LCF are relatively subtle.

Clearly, the properties of the perovskite do matter, as shown by the fact that cathodes formed by infiltration of LSM into similar porous YSZ scaffolds exhibit significantly higher impedances than the series of $LaFeO_3$-based materials investigated here [43]. LSM has a similar electronic conductivity as LNF but has much lower ionic conductivity, reportedly 4×10^{-8} S cm^{-1} at 800 °C [46]. Comparing the various $LaFeO_3$-based materials from the present study, the open-circuit impedances appear to also decrease with increasing ionic conductivity, but with a very weak dependence. Of the materials tested, LSF has the highest ionic conductivity by a significant margin and shows the lowest open-circuit impedance after calcination to 1100 °C. However, it must be acknowledged that the electrochemical performance of all the $LaFeO_3$-based perovskites studied here was similar, even though the ionic conductivity at 700 °C varied from 1.6×10^{-6} S cm^{-1} for LNF to 8.3×10^{-4} S cm^{-1} for LSF.

The catalytic properties of the perovskites in the $LaFeO_3$ series do not appear to be of critical importance. If they were, one would expect that the Ni-containing material to be much more effective at reducing O_2, given that Ni is much more easily reduced than Fe. Since cathode performance is likely limited by diffusion in our study, at least following calcination to 1100 °C, it is possible that the lack of dependence on catalytic properties is associated with our particular operating regime. However, while there is an extensive literature involving attempts to improve the electrochemical properties of SOFC cathodes by adding catalytic promoters, a recent review of this literature also suggested that there is no clear-cut evidence for a relationship between performance and the addition of catalytic components [17].

It is interesting to ask what gives rise to the current-dependent impedance in the electrodes calcined to higher temperatures. While it is possible that solid-state reactions between the perovskites and the YSZ lead to the formation of interfacial compounds in quantities too small to observe with XRD, the formation of insulating layers would be expected to influence the ohmic losses in the cell, rather than the non-ohmic losses. Furthermore, it seems unlikely to us that formation of compounds like $La_2Zr_2O_7$ would be reversed by electrode polarization. In previous studies, it has been suggested that the curvature in the *V–I* relationship could be associated with ion diffusion through the perovskite film and coupling of that diffusion process with diffusion of oxygen ions through the YSZ scaffold [20]. Alternatively, diffusion of oxygen ions in the perovskite mixed conductor could have concentration and field dependences [34], so that the effective diffusivity could be nonlinear. Either of these mechanisms would explain changes in the impedance with ionic conductivity, although one would expect the dependence to be stronger than we observed here. Evidence for a diffusion process limiting electrode performance comes from the low peak frequencies in the impedance spectra of the deactivated electrodes. Also, the potential gradients across a film would be similar for both anodic and cathodic polarization, so that the electrode impedance should be affected in a similar manner for cathodic and anodic polarization for a diffusional process.

While the performances of the LNF and LSNF electrodes are excellent following low-temperature calcination, essentially the same as that of LSF, it is doubtful that this level of performance will be stable. In the earlier studies of LSF–YSZ composites, it was shown that operation at 700 and 800 °C for several thousand hours caused changes in the electrode that were similar to those caused by calcination to 1100 °C [20]. Therefore, the performance of the electrode following high-temperature calcination is probably more indicative of that which would be observed during much of the lifetime of fuel cells made with these materials.

As we pointed out in Section 1, one of the problems with LSF cathodes is their relatively poor electronic conductivity, a problem that is solved with electrodes based on LNF and LSNF. If methods can be developed to prevent sintering and film formation, the properties of these new perovskites appear to be quite attractive.

5. Conclusions

The properties LNF–YSZ and LSNF–YSZ composite electrodes formed by infiltration were investigated. Based on XRD, solid-state reactions between the perovskite and the YSZ do not appear to be a problem for practical operating temperatures. The electrochemical properties following calcination at lower temperatures are very good but higher calcination temperatures cause the perovskites to form a film over the YSZ scaffold that appears to limit performance. It is suggested that a method to prevent film formation would result in SOFC cathodes with outstanding properties.

Acknowledgements

This work was funded by the U.S. Department of Energy's Hydrogen Fuel Initiative (grant DE-FG02-05ER15721). PF and MB thanks FISR-MUR (Rome) grant 'Inorganic and Hybrid Nanosystems for the Development and Innovation of Fuel Cells' for financial support.

References

[1] F. Tietz, Q. Fu, V.A.C. Haanappel, A. Mai, N.H. Menzler, S. Uhlenbruck, Int. J. Appl. Ceram. Technol. 4 (2007) 436.
[2] S.B. Adler, Chem. Rev. 104 (2004) 4791.
[3] J. Fleig, J. Maier, J. Eur. Ceram. Soc. 24 (2004) 1343.
[4] N.Q. Minh, J. Am. Ceram. Soc. 76 (1993) 563.
[5] A. Mineshige, M. Kobune, S. Fujii, Z. Ogumi, M. Inaba, T. Yao, K. Kikuchi, J. Solid State Chem. 142 (1999) 374.
[6] H. Uchida, S. Arisaka, M. Watanabe, Solid State Ionics 135 (2000) 347.
[7] T. Horita, K. Yamaji, N. Sakai, H. Yokokawa, A. Weber, E. Ivers-Tiffee, Electrochim. Acta 46 (2001) 1837.
[8] S.J. Skinner, Int. J. Inorg. Mater. 3 (2001) 113.
[9] J.M. Ralph, C. Rossignol, R. Kumar, J. Electrochem. Soc. 150 (2003) A1518.
[10] S.P. Simner, J.F. Bonnett, N.L. Canfield, K.D. Meinhardt, V.L. Sprenkle, J.W. Stevenson, Electrochem. Solid-State Lett. 5 (2002) A173.
[11] S.P. Simner, J.F. Bonnett, N.L. Canfield, K.D. Meinhardt, J.P. Shelton, V.L. Sprenkle, J.W. Stevenson, J. Power Sources 113 (2003) 1.
[12] Y. Huang, J.M. Vohs, R.J. Gorte, J. Electrochem. Soc. 151 (2004) A646.
[13] A. Esquirol, N.P. Brandon, J.A. Kilner, M. Mogensen, J. Electrochem. Soc. 151 (2004) A1847.
[14] S.P. Jiang, Solid State Ionics 146 (2002) 1.
[15] Y. Huang, K. Ahn, J.M. Vohs, R.J. Gorte, J. Electrochem. Soc. 151 (2004) A1592–A1597.
[16] H. He, Y. Huang, J. Regal, M. Boaro, J.M. Vohs, R.J. Gorte, J. Am. Ceram. Soc. 87 (2004) 331.
[17] J.M. Vohs, R.J. Gorte, Adv. Mater. 21 (2009) 943–956.
[18] M. Sase, D. Ueno, K. Yashiro, A. Kaimai, T. Kawada, J. Mizusaki, J. Phys. Chem. Solids 66 (2005) 343.
[19] Y. Huang, J.M. Vohs, R.J. Gorte, J. Electrochem. Soc. 153 (2006) A951.
[20] W. Wang, M.D. Gross, J.M. Vohs, R.J. Gorte, J. Electrochem. Soc. 154 (2007) B439.
[21] S.P. Simner, J.P. Shelton, M.D. Anderson, J.W. Stevenson, Solid State Ionics 161 (2003) 11.
[22] M. Bevilacqua, T. Montini, C. Tavagnacco, E. Fonda, P. Fornasiero, M. Graziani, Chem. Mater. 19 (2007) 5926.
[23] M. Bevilacqua, T. Montini, C. Tavagnacco, G. Vicario, P. Fornasiero, M. Graziani, Solid State Ionics 177 (2006) 2957.
[24] T. Montini, M. Bevilacqua, E. Fonda, M.F. Casula, S. Lee, C. Tavagnacco, R.J. Gorte, P. Fornasiero, Chem. Mater. 21 (2009) 1768.
[25] S.-W. Jung, J.M. Vohs, R.J. Gorte, J. Electrochem. Soc. 154 (2007) B1270.
[26] R. Chiba, F. Yoshimura, Y. Sakurai, Solid State Ionics 124 (1999) 281.
[27] T. Komatsu, R. Chiba, H. Arai, K. Sato, J. Power Sources 176 (2008) 132.
[28] Y.D. Zhen, A.I.Y. Tok, S.P. Jiang, F.Y.C. Boey, J. Power Sources 170 (2007) 61.
[29] R. Chiba, T. Komatsu, Y. Tabata, H. Orui, K. Nozawa, H. Arai, M. Arakawa, Solid State Ionics 178 (2008) 1701.
[30] H. Orui, K. Watanabe, R. Chiba, M. Arakawa, J. Electrochem. Soc. 151 (2004) A1412.
[31] R. Chiba, T. Komatsu, H. Orui, H. Taguchi, K. Nozawa, H. Arai, Electrochem. Solid-State Lett. 12 (2009) B69.
[32] G.W. Coffey, J.S. Hardy, L.R. Pederson, P.C. Rieke, E.C. Thomsen, Electrochem. Solid-State Lett. 6 (2003) A121.
[33] R.J. Gorte, S. Park, J.M. Vohs, C. Wang, Adv. Mater. 12 (2000) 1465.
[34] F. Bidrawn, S. Lee, J.M. Vohs, R.J. Gorte, J. Electrochem. Soc. 155 (2008) B660.
[35] S. Park, R.J. Gorte, J.M. Vohs, J. Electrochem. Soc. 148 (2001) A443.
[36] M. Boaro, J.M. Vohs, R.J. Gorte, J. Am. Ceram. Soc. 86 (2003) 395.
[37] M.D. Gross, J.M. Vohs, R.J. Gorte, J. Electrochem. Soc. 154 (2007) B694.
[38] M.D. Gross, J.M. Vohs, R.J. Gorte, Electrochem. Solid-State Lett. 10 (2007) B65.
[39] G. Kim, J.M. Vohs, R.J. Gorte, J. Mater. Chem. 18 (2008) 2386–2390.
[40] S. McIntosh, J.M. Vohs, R.J. Gorte, J. Electrochem. Soc. 150 (2003) A1305.
[41] H. Falcon, A.E. Goeta, G. Punte, R.E. Carbonio, J. Solid State Chem. 133 (1997) 379.
[42] H. Yokokawa, H. Tu, B. Iwanschitz, A. Mai, J. Power Sources 182 (2008) 400.
[43] Y.Y. Huang, J.M. Vohs, R.J. Gorte, J. Electrochem. Soc. 152 (2005) A1347–A1353.
[44] Y. Huang, J.M. Vohs, R.J. Gorte, Electrochem. Solid-State Lett. 9 (2006) A237–A240.
[45] L.Y. Woo, R.S. Glass, R.J. Gorte, C.A. Orme, A.J. Nelson, J. Electrochem. Soc. 156 (2009) B602.
[46] Y. Ji, J.A. Kilner, M.F. Carolan, Solid State Ionics 176 (2005) 937.